



High Densification Level and Hardness Values of Additively Manufactured 316L Stainless Steel Fabricated by Fused Filament Fabrication

Nur Hidayah Musa¹, Nurainaa Mazlan¹, Shahir Mohd Yusuf^{1,*}, Nur Azmah Nordin¹, Saiful Amri Mazlan¹, Nong Gao²

¹ Engineering Materials and Structures (eMast) iKohza, Malaysia–Japan International Institute of Technology (MJIT), Universiti Teknologi Malaysia, Jalan Sultan Yahya Petra, 54100 Kuala Lumpur, Malaysia

² Materials Research Group, Faculty of Engineering and Physical Sciences, University of Southampton, Southampton SO17 1BJ, United Kingdom

ARTICLE INFO

Article history:

Received 7 July 2023

Received in revised form 10 November 2023

Accepted 19 November 2023

Available online 6 December 2023

Keywords:

Additive manufacturing; fused filament fabrication; 316L stainless steel; densification level; hardness

ABSTRACT

Laser powder bed fusion (L-PBF) has emerged as the most widely used additive manufacturing (AM) process, also known as 3D printing, to fabricate 316L stainless steel (316L SS) components for various applications. However, the initial setup, operation, and maintenance costs are too expensive due to the complex machinery, high energy-consuming laser beam, and proprietary software required. Therefore, in this paper, fused filament fabrication (FFF) is proposed as a low-cost AM approach to fabricate 316L SS specimens via a 3-step printing-debinding-and sintering process. The specimens are initially printed on a desktop FFF AM 3D printer by varying nozzle temperatures from 195 – 220°C, followed by debinding up to 427°C for 4 hours, and finally sintering at 1260°C for 4 hours. The results show that nozzle temperature 200°C yielded the highest densification level of 97.6% and highest average hardness value of 292 HV, indicating that 3D printing parameters, particularly nozzle temperature plays an important role in influencing the properties of the sintered specimens. Overall, the results from this study prove that FFF is a viable and cost-effective AM process that has the potential to produce 316L SS parts that meet industrial requirements.

1. Introduction

Powder bed fusion (PBF) is a well-established additive manufacturing (AM) process to produce metallic materials with complex and intricate features and tailorable microstructures to suit respective applications. This process involves the selective melting and fusing of successive powder layers to produce complete 3D objects according to the initial computer aided design (CAD) file. However, L-PBF AM processes such as selective laser melting (SLM) and direct metal laser sintering (DMLS) require expensive machinery and materials (upwards of \$80,000), laser beam heat source that consumes a lot of energy, and proprietary hardware and software, which are difficult to operate and therefore not easily accessible [1-4]. These result in unavoidably high investment and

* Corresponding author.

E-mail address: shahiryasin@utm.my

<https://doi.org/10.37934/araset.34.2.144152>

maintenance costs that are prohibitive to numerous academic institutions and even certain industries.

However, recently, fused filament fabrication (FFF), an AM technology under the material extrusion category has emerged as a viable and cost-effective approach to process metallic materials, primarily 316L SS due to its widespread application in the biomedical, marine, and petrochemical industries [5-9]. This method can be executed by using the widely available commercial desktop FFF AM machines, also called 3D printers, and the accompanying open-source software through a 3-stage printing-debinding-sintering process. Nowadays, decent desktop FFF AM 3D printers that can process numerous polymer materials can be purchased for <\$1,000, and the same 3D printers have been shown to be capable of processing metallic materials [7,10,11]. It is estimated that successful part fabrication via desktop FFF AM 3D printers can significantly reduce the overall cost of production of metallic components through metal AM technology from \$500,000 to merely \$500 [12].

In the printing process, filaments containing metal-polymer binder mix are fed into a heated nozzle that is then extruded onto a print bed layer-by-layer upon completion of a 3D object based on the CAD input. The feedstock material for the filaments can be synthesized from readily available powders and binders that are used for powder metallurgy (PM) and metal injection molding (MIM) process, which is relatively more affordable compared to the metal powders used for L-PBF AM techniques [4,13,14]. This is because the whole sequence of FFF AM can be considered similar as PM and MIM due to the debinding and sintering requirements to produce fully dense metallic parts. The only difference is the initial compacting and moulding stage in PM and MIM, respectively is replaced by 3D printing, which offers more design flexibility and complexity due to the layer-wise and freeform shaping approach. Therefore, a myriad of technical references in FFF AM can be based on the established PM and MIM, particularly for optimising the debinding and sintering parameters to attain fully dense metallic parts [15-17]. Furthermore, the important processing parameters of FFF AM process that need to be controlled, particularly nozzle temperature, print speed, and infill density can be easily adjusted and controlled by using free and open-source 'slicing' software such as Cura that can be freely downloaded from the internet, unlike the proprietary L-PBF counterpart. Subsequently, the as-printed part, termed 'green' part is subjected to a debinding process to remove the binder materials, and is now known as 'brown' part. The 'brown' part is then sintered for further consolidation into the finished part. Studies have shown that the sintered part can achieve up to 98% densification level (with respect to the theoretical density of the respective materials), which is similar to those attained in PM, MIM and L-PBF AM processes, highlighting the feasibility of FFF AM technique to produce metallic parts and the potential to be applied for industrial applications [8,10].

However, most studies on FFF AM of 316L SS have focused on optimising the sintering parameters and/or post-processing to achieve the highest attainable densification level in the sintered parts [5-9]. Not many researchers investigated the influence of 3D printing parameters on the properties of the sintered parts, except for one study by Caminero *et al.*, [3] whom investigated the effect of build orientation on the tensile strength of FFF AM 316L SS parts. Thus, an opportunity arises to tailor the properties of FFF AM 316L SS by manipulating 3D printing parameters at the initial printing stage itself, rather than during the later sintering stage. Therefore, in this study, FFF AM 316L SS specimens were manufactured by varying the nozzle temperatures during the 3D printing process, followed by debinding and sintering using constant parameters. Subsequently, the densification level and hardness of the sintered specimens were evaluated by Archimedes method and Vickers hardness (HV) measurements, respectively to determine the influence of nozzle temperatures (3D printing parameter) on the mechanical properties of 316L SS fabricated by FFF AM process.

2. Methodology

2.1 Material

The filament material used in this study was a 316L SS – PLA (metal-polymer binder) mixture with a high metal loading of 87.5 wt.% having a circular cross-section of 1.75 mm, purchased from The Virtual Foundry, TVF (USA). The chemical composition of the filament as given by the supplier is as follows (in wt.%): Silicon: 0.3-0.75, Manganese: 1.8-2.0, Sulphur: <0.03, Phosphorus: <0.04, Chromium: 16-18, Nickel: 10-14, Molybdenum: 2-3, Iron: *bal.*, PLA: 12.5, and binding additive: trace.

2.2 Specimen Fabrication, Debinding, and Sintering

A direct-drive desktop FFF AM 3D printer, Artillery Sidewinder X1 (Evnovo, China) was used to print 25 x 25 x 25 mm cubes, which was initially designed in SolidWorks. Hardened steel nozzle was used for the 3D printing process due to its ability to withstand high abrasion from the abrasive metal powders in the filament. The initial 3D printing parameters used in this study were based on those recommended by TVF, as follows: nozzle temperature, T_n : 190°C, print bed temperature, T_b : 60°C, infill density, ρ_i : 100%, and infill flow rate, f_i : 100%, layer height, h : 0.2 mm, nozzle diameter, d : 0.4 mm, raster infill pattern, and cooling fan switched off. Preliminary tests of extruding 10 layers were carried out using these parameters, but they were unsuccessful as the nozzle became clogged, and no material was extruded out of the nozzle. Thus, the nozzle temperature was increased with an increment of 10°C in subsequent test runs. The printing process of 10 test layers was successful up to 220°C with excellent layer adhesion on the print bed, after which the nozzle was again clogged without any filament extrusion. Hence, the nozzle temperatures were varied from 195°C to 220°C in 5°C increments to proceed with the fabrication of complete cubes as required while the other parameters were kept constant.

The 3D printed cubes, so-called 'green parts' were then subjected to a thermal debinding process inside an electrical chamber furnace (model LH 30/14 by Nabertherm GmbH, Lilienthal, Germany) to remove the polymer binder content in the green part. The temperature inside the furnace was ramped up to 204°C at a rate of 1°C/min and then held for 2 hours before being ramped again to 427°C at 1°C/min and held for another 2 hours. After debinding, the debound cubes, now termed 'brown parts' were directly sintered inside the same furnace at 1260°C for a holding time of 4 hours. After that, the brown parts, now known as sintered/final part were left inside the furnace to be air-cooled down to room temperature.

2.3 Densification Level Evaluation and Hardness Measurements

The density of the final parts was determined by using Archimedes principle based on ASTM B 962-08 standard via the following equation

$$\rho = \frac{W_0 \rho_f}{W_0 - W_i} \quad (1)$$

where W_0 is the weight of the object in air, W_i is the weight of object when immersed in fluid (water in this case) and ρ_f is the density of fluid (1 g/cm³ for water). Subsequently, the densification level (relative density) of the final parts was determined by dividing the measured density of the cubes using Eq. (1) with the theoretical density of 316L SS (8 g/cm³). The calculated densification level values for FFF AM-produced 316L SS are then displayed as percentages (%) with respect to the theoretical density of 316L SS.

The hardness of the final parts was evaluated through Vickers microhardness (HV) measurements taken at ≥ 30 different locations throughout the cross-section and surface cut parallel to the print bed (surface-parallel) of the cubes under a load of 100 gf and a dwell time of 15 s.

3. Results and Discussion

3.1 Printing Results

The green parts produced after 3D printing of the cubes at various nozzle temperatures are shown by representative images in Figure 1. It is clear that more excess material is extruded on the sides of the cubes with increasing nozzle temperature from 210°C to 220°C (Figure 1(b)-(d)), which is caused by the excess melting of the filament material that accumulates at the tip of the nozzle before being attached to the cubes during the extrusion process. On the other hand, cubes with consistent shape and dimensions as the CAD file are produced without any excess material or shrinkage when the nozzle temperature is set at 200°C as shown in Figure 1(a). It should be mentioned that similarly perfect cubes were also attained at $T_n=195^\circ\text{C}$ and 205°C , which suggest that 195 – 205°C are the optimum range of nozzle temperatures to 3D print high quality specimens from 316L SS filaments with high structural and dimensional integrity. However, the excess material is actually only loosely attached to the surface of the cubes and can be removed just by using knife, files, or other deburring tools similar to those done to those on 3D printed polymer parts. Nevertheless, for strict quality measures, 195 – 205°C are the recommended nozzle temperatures to print this material.

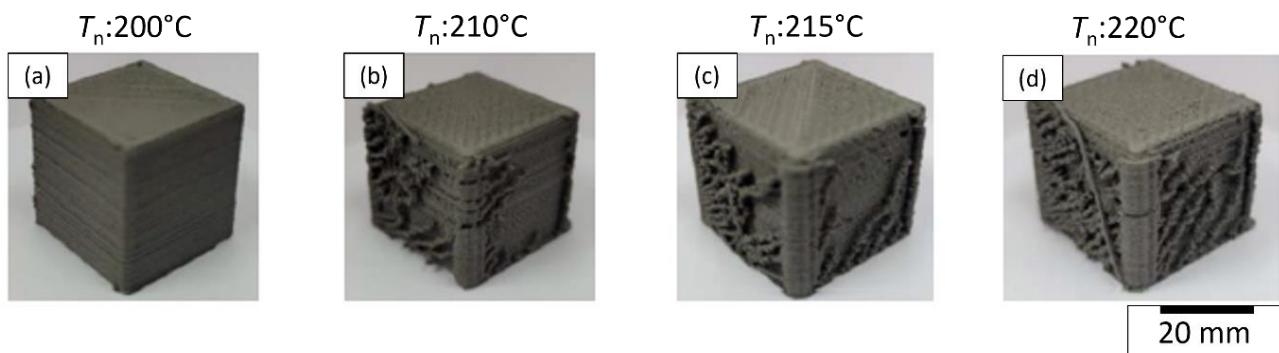


Fig. 1. Green parts after 3D printing at different nozzle temperatures

On the other hand, representative images of the corresponding sintered parts are shown in Figure 2, in which several observations can be made here. Firstly, the surfaces of the cubes seem to be increasingly porous as indicated by the higher amounts of visible voids with increasing nozzle temperatures from 210°C to 220°C (Figure 2(b)-(d)), while $T_n=200^\circ\text{C}$ yields the most visibly solid surface with less amount and smaller-sized voids. Secondly, the dimensional integrity was not maintained after sintering for all samples, in which all of them suffered from bulging at the centre to lower-half portion of the cubes by about 10%. The sintered part at $T_n=200^\circ\text{C}$ and 210°C exhibit 'stair-shaped' bulging, while those at $T_n=215^\circ\text{C}$ and 220°C display 'A-shaped' bulging, which are known distortion modes that are also observed in other sintered metals and alloys [20,21]. Such distortions are typically attributed to the sintering environment, e.g. air, argon, or vacuum, sintering pressure, or porosity that are present within the samples during the sintering process [22,23].

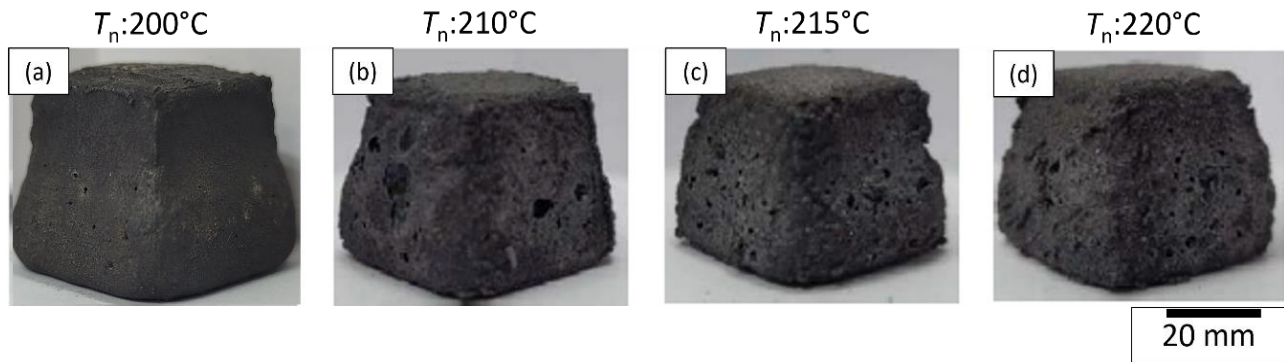


Fig. 2. Appearance of sintered parts initially 3D printed at different nozzle temperatures

3.2 Evaluation of Densification Level

Table 1 displays the actual density measured from the sintered parts and the overall densification level (relative density) measured with respect to the theoretical density of 316L SS. On the other hand, Figure 3 visualises the trend of variation in relative density for sintered samples that were initially 3D printed with different nozzle temperatures. An interesting trend of increasing relative density is observed when the nozzle temperatures are increased from 195°C to 200°C before gradually decreasing beyond 200°C based on the results in Table 1 and Figure 3.

Table 1

Measured density and relative density of the sintered parts for different nozzle temperatures

T_n (°C)	Measured density (g/cm ³)	Relative density (%)
195	6.552	81.9
200	7.786	97.6
205	5.320	66.4
210	4.693	58.7
215	4.640	58.1
220	4.604	57.6

The highest relative density of 97.6% is attained at a nozzle temperature of 200°C, suggesting that this is the best nozzle temperature that can yield the highest relative density within the recommended range of 195 – 205°C mentioned previously. Such high relative density is comparable to metallic materials fabricated by other metal AM techniques such as SLS and conventional MIM and PM processes [3,6-10], which would make it possible for the FFF AM-fabricated 316L SS to be applied for various industrial applications [24].

Figure 4 exhibits the surface-parallel of the sintered parts resulting from 3D printing at nozzle temperatures ranging from 195 – 205°C. Small and deep voids with several short lines can be seen on the surface of $T_n=195^\circ\text{C}$ (Figure 4(a)), which correspond to porosity due to unsintered metal filament and defects resulting from inadequate adhesion among the raster infill patterns [8]. On the other hand, no voids are observed for $T_n=200^\circ\text{C}$ (Figure 4(b)), with the raster infill pattern defects are also minimised. However, the surface-parallel for $T_n=205^\circ\text{C}$ (Figure 4(c)) clearly shows increased amounts of deep voids and raster defects. These observations correlate well with the trend of increasing relative density from $T_n=195^\circ\text{C}$ to $T_n=200^\circ\text{C}$, and its decrease at $T_n=205^\circ\text{C}$ (Table 1 and Figure 3), suggesting an inverse relationship between void and defect contents with relative density (the higher the number of voids and defects, the lower the relative density of a sintered material)

[17,25-27]. This phenomenon could be caused by inadequate sintering time, resulting in reduced diffusion among the metal powder particles, leaving areas of unfused material manifesting as voids/defects [26].

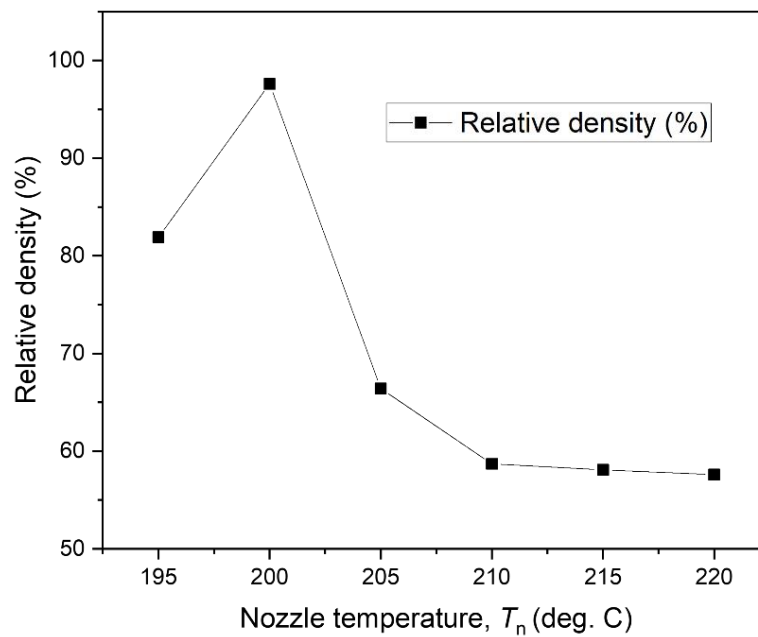


Fig. 3. Graph of relative density of the sintered parts against nozzle temperatures used to 3D print the samples initially

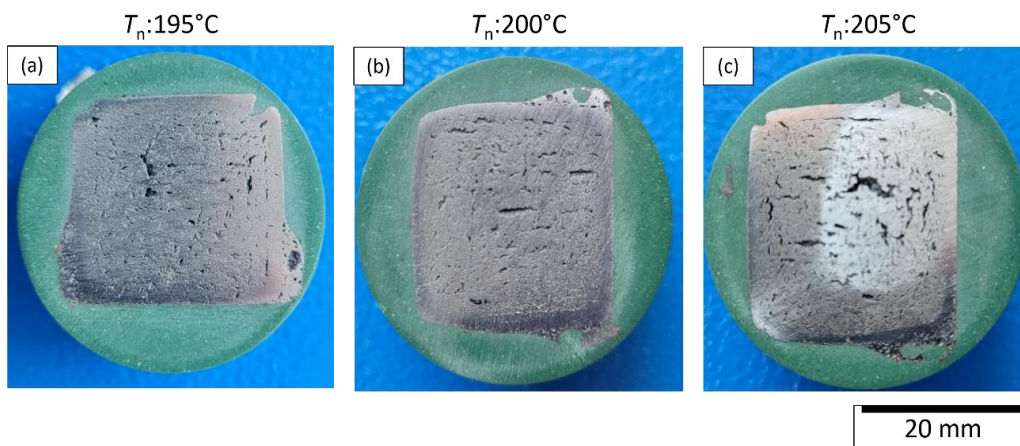


Fig. 4. Cross-section of sintered parts that was initially subjected to 3D printing at different nozzle temperatures

3.3 Hardness Measurements

The average hardness values of the sintered parts for nozzle temperatures 195°C to 205°C are shown in Table 2. The trend of hardness variation follows that of the relative density shown in Table 1 and Figure 3, in which $T_n=200^\circ\text{C}$ yields the highest HV value (292 HV), followed by $T_n=195^\circ\text{C}$ (270 HV), and the lowest hardness is 160 HV that is attained at $T_n=205^\circ\text{C}$. It is obvious that high void/defect contents lead to low hardness due to their collapse within the solid material under loading [18] and vice versa, as is the case for other materials subjected to sintering/melting and solidification processes [28-31]. The results of hardness values of sintered parts for $T_n=195^\circ\text{C}$ (relative density:

81.9%, hardness: 270 HV) and 200°C (relative density: 97.6%, hardness: 292 HV) are higher than those obtained in other studies of 316L SS fabricated by FFF AM and conventional PM and MIM processes reported in literature, ~100 – 175 HV [3,6-10], which can be attributed to the high volume fraction of metal powder (metal loading) of 87.5 wt.% used in this study compared to 50 – 80 wt.% used in those studies. Such high metal loading has been found to result in more metallic powder particles to be sintered per unit area, i.e. high compaction, thereby leading to generation of more grain boundaries that become effective sites to impede dislocation density [32,33]. However, the HV value of sintered parts for $T_n=205^\circ\text{C}$ (relative density: 66.4%) significantly decreases to 160 HV, which suggests that the negative consequence of voids and defects overcome the benefits of using high metal loading for FFF AM 316L SS in this study [28]. Thus, based on the results in this study, it could be reasonably inferred that increasing metal loadings would yield higher hardness values in parts subjected to sintering process provided that the void/defect content is <20%. Nevertheless, despite the promising hardness results, further mechanical testing through tensile tests is necessary to discuss the mechanical properties more comprehensively in the future [34-36].

Table 2
HV values of the sintered parts for different nozzle temperatures

T_n (°C)	Vickers microhardness (HV)
195	270 ± 20
200	292 ± 34
205	160 ± 25

4. Conclusions

In this study, 316L SS specimens were fabricated using FFF AM process using filament feedstock material with high metal loading (87.5 wt.%) by varying the nozzle temperatures from 195 – 205°C, followed by debinding and sintering to remove the polymer binder and produce fully dense metallic parts. Subsequently, the densification level and hardness values of the sintered specimens were determined through Archimedes method (ASTM B 962-08) and Vickers microhardness (HV) measurements, respectively. The results show that 200°C is the best nozzle temperature that produces sintered specimens having the highest relative density of 97.6% and highest average HV value of 292 HV. This implies that 3D printing parameters (nozzle temperature) also has an important role in determining the properties of FFF AM parts, and not only the sintering parameters. Overall, the results from this study prove the feasibility of FFF AM process to manufacture cost-effective metallic components for various engineering applications, although further research is required particularly on maintaining the structural and dimensional integrity of the parts after sintering.

Acknowledgement

This research was funded by the Ministry of Higher Education (MOHE) Malaysia through the Fundamental Research Grant Scheme (FRGS /1/2021/TK0/UTM/02/84).

References

- [1] Gong, Haijun, Dean Snelling, Kamran Kardel, and Andres Carrano. "Comparison of stainless steel 316L parts made by FDM-and SLM-based additive manufacturing processes." *Jom* 71 (2019): 880-885. <https://doi.org/10.1007/s11837-018-3207-3>
- [2] Damon, James, Stefan Dietrich, Sasidhar Gorantla, Uwe Popp, Brando Okolo, and Volker Schulze. "Process porosity and mechanical performance of fused filament fabricated 316L stainless steel." *Rapid Prototyping Journal* 25, no. 7 (2019): 1319-1327. <https://doi.org/10.1108/RPJ-01-2019-0002>

- [3] Caminero, Miguel Ángel, Ana Romero, Jesús Miguel Chacón, Pedro José Núñez, Eustaquio García-Plaza, and Gloria Patricia Rodríguez. "Additive manufacturing of 316L stainless-steel structures using fused filament fabrication technology: Mechanical and geometric properties." *Rapid Prototyping Journal* 27, no. 3 (2021): 583-591. <https://doi.org/10.1108/RPJ-06-2020-0120>
- [4] Godec, Damir, Santiago Cano, Clemens Holzer, and Joamin Gonzalez-Gutierrez. "Optimization of the 3D printing parameters for tensile properties of specimens produced by fused filament fabrication of 17-4PH stainless steel." *Materials* 13, no. 3 (2020): 774. <https://doi.org/10.3390/ma13030774>
- [5] Thompson, Yvonne, Joamin Gonzalez-Gutierrez, Christian Kukla, and Peter Felfer. "Fused filament fabrication, debinding and sintering as a low cost additive manufacturing method of 316L stainless steel." *Additive Manufacturing* 30 (2019): 100861. <https://doi.org/10.1016/j.addma.2019.100861>
- [6] Tosto, Claudio, Jacopo Tirillò, Fabrizio Sarasini, and Gianluca Cicala. "Hybrid metal/polymer filaments for fused filament fabrication (FFF) to print metal parts." *Applied Sciences* 11, no. 4 (2021): 1444. <https://doi.org/10.3390/app11041444>
- [7] Wang, Yun, Li Zhang, Xun Li, and Zhao Yan. "On hot isostatic pressing sintering of fused filament fabricated 316L stainless steel—evaluation of microstructure, porosity, and tensile properties." *Materials Letters* 296 (2021): 129854. <https://doi.org/10.1016/j.matlet.2021.129854>
- [8] Santamaria, Ricardo, Mobin Salasi, Sam Bakhtiari, Garry Leadbeater, Mariano Iannuzzi, and Md Zakaria Quadir. "Microstructure and mechanical behaviour of 316L stainless steel produced using sinter-based extrusion additive manufacturing." *Journal of Materials Science* (2022): 1-17. <https://doi.org/10.1007/s10853-021-06828-8>
- [9] Burkhardt, Carlo, Peter Freigassner, Oxana Weber, Philipp Imgrund, and Stefan Hampel. "Fused filament fabrication (FFF) of 316L Green Parts for the MIM process." *World PM2016-AM-Deposition Technologies* (2016).
- [10] Nurhudan, Aghnia Ilmiah, Sugeng Supriadi, Yudan Whulanza, and Agung Shamsuddin Saragih. "Additive manufacturing of metallic based on extrusion process: A review." *Journal of Manufacturing Processes* 66 (2021): 228-237. <https://doi.org/10.1016/j.jmapro.2021.04.018>
- [11] Tabares, Eduardo, Michael Kitzmantel, Erich Neubauer, Antonia Jimenez-Morales, and Sophia A. Tsipas. "Extrusion-based additive manufacturing of Ti3SiC2 and Cr2AlC MAX phases as candidates for high temperature heat exchangers." *Journal of the European Ceramic Society* 42, no. 3 (2022): 841-849. <https://doi.org/10.1016/j.jeurceramsoc.2021.10.042>
- [12] Warriar, Nirupama, and Kunal H. Kate. "Fused filament fabrication 3D printing with low-melt alloys." *Progress in Additive Manufacturing* 3, no. 1-2 (2018): 51-63. <https://doi.org/10.1007/s40964-018-0050-6>
- [13] Liu, Bin, Yuxiang Wang, Ziwei Lin, and Tao Zhang. "Creating metal parts by fused deposition modeling and sintering." *Materials Letters* 263 (2020): 127252. <https://doi.org/10.1016/j.matlet.2019.127252>
- [14] Sames, William J., F. A. List, Sreekanth Pannala, Ryan R. Dehoff, and Sudarsanam Suresh Babu. "The metallurgy and processing science of metal additive manufacturing." *International materials reviews* 61, no. 5 (2016): 315-360. <https://doi.org/10.1080/09506608.2015.1116649>
- [15] Singh, Gurminder, Jean-Michel Missiaen, Didier Bouvard, and Jean-Marc Chaix. "Additive manufacturing of 17-4 PH steel using metal injection molding feedstock: Analysis of 3D extrusion printing, debinding and sintering." *Additive Manufacturing* 47 (2021): 102287. <https://doi.org/10.1016/j.addma.2021.102287>
- [16] Sun, Pei, Z. Zak Fang, Yang Xia, Ying Zhang, and Chengshang Zhou. "A novel method for production of spherical Ti-6Al-4V powder for additive manufacturing." *Powder Technology* 301 (2016): 331-335. <https://doi.org/10.1016/j.powtec.2016.06.022>
- [17] Verlee, Bruno, Thierry Dormal, and Jacqueline Lecomte-Beckers. "Density and porosity control of sintered 316L stainless steel parts produced by additive manufacturing." *Powder Metallurgy* 55, no. 4 (2012): 260-267. <https://doi.org/10.1179/0032589912Z.00000000082>
- [18] Cherry, J. A., H. M. Davies, S. Mehmood, N. P. Lavery, S. G. R. Brown, and JTIJoAMT Sienz. "Investigation into the effect of process parameters on microstructural and physical properties of 316L stainless steel parts by selective laser melting." *The International Journal of Advanced Manufacturing Technology* 76 (2015): 869-879. <https://doi.org/10.1007/s00170-014-6297-2>
- [19] Tucho, Wakshum M., Vidar H. Lysne, Håkon Austbø, Atle Sjolyst-Kverneland, and Vidar Hansen. "Investigation of effects of process parameters on microstructure and hardness of SLM manufactured SS316L." *Journal of Alloys and Compounds* 740 (2018): 910-925. <https://doi.org/10.1016/j.jallcom.2018.01.098>
- [20] Mousapour, Mehrdad, Maziyar Azadbeh, and Herbert Danninger. "Effect of compacting pressure on shape retention during supersolidus liquid phase sintering of Cu base alloys." *Powder Metallurgy* 60, no. 5 (2017): 393-403. <https://doi.org/10.1080/00325899.2017.1357781>
- [21] Ghasemi, Somayeh, Maziyar Azadbeh, Mehrdad Mousapour, Ahad Mohammadzadeh, Herbert Danninger, and Nushin Salimi. "The role of pore evolution during supersolidus liquid phase sintering of prealloyed brass powder." *Powder Metallurgy* 63, no. 3 (2020): 187-196. <https://doi.org/10.1080/00325899.2020.1785155>

- [22] Lu, Peizhen, Xiaoping Xu, Wuwen Yi, and Randall M. German. "Porosity effect on densification and shape distortion in liquid phase sintering." *Materials Science and Engineering: A* 318, no. 1-2 (2001): 111-121. [https://doi.org/10.1016/S0921-5093\(01\)01330-2](https://doi.org/10.1016/S0921-5093(01)01330-2)
- [23] Manière, Charles, Elia Saccardo, Geuntak Lee, Joanna McKittrick, Alberto Molinari, and Eugene A. Olevsky. "Swelling negation during sintering of sterling silver: An experimental and theoretical approach." *Results in Physics* 11 (2018): 79-84. <https://doi.org/10.1016/j.rinp.2018.08.035>
- [24] Roshchupkin, Stanislav, Alexander Kolesov, Alexey Tarakhovskiy, and Ivan Tishchenko. "A brief review of main ideas of metal fused filament fabrication." *Materials Today: Proceedings* 38 (2021): 2063-2067. <https://doi.org/10.1016/j.matpr.2020.10.142>
- [25] Kurgan, Naci. "Effect of porosity and density on the mechanical and microstructural properties of sintered 316L stainless steel implant materials." *Materials & Design* 55 (2014): 235-241. <https://doi.org/10.1016/j.matdes.2013.09.058>
- [26] Almomani, Mohammed A., Ahmad M. Shatnawi, and Mohammed K. Alrashdan. "Effect of sintering time on the density, porosity content and microstructure of copper–1 wt.% silicon carbide composites." *Advanced Materials Research* 1064 (2015): 32-37. <https://doi.org/10.4028/www.scientific.net/AMR.1064.32>
- [27] Lu, Zhen, Zhenhan Huang, Shaosong Jiang, Wei Liu, and Kaifeng Zhang. "Influencing factors for the microstructure and mechanical properties of micro porous titanium manufactured by metal injection molding." *Metals* 6, no. 4 (2016): 83. <https://doi.org/10.3390/met6040083>
- [28] Liu, Yingying, Sheng Ge, Yihua Huang, Zhengren Huang, and Deku Zhang. "Influence of sintering process conditions on microstructural and mechanical properties of boron carbide ceramics synthesized by spark plasma sintering." *Materials* 14, no. 5 (2021): 1100. <https://doi.org/10.3390/ma14051100>
- [29] Kaku, Sai Mahesh Yadav, Asit Kumar Khanra, and M. J. Davidson. "Effect of deformation on densification and corrosion behavior of Al-ZrB₂ composite." *Metallurgical and Materials Engineering* 23, no. 1 (2017): 47-63. <https://doi.org/10.30544/264>
- [30] Kim, Yunsung, Hyungyung Jo, Jan L. Allen, Heeman Choe, Jeff Wolfenstine, and Jeff Sakamoto. "The effect of relative density on the mechanical properties of hot-pressed cubic Li₇La₃Zr₂O₁₂." *Journal of the American Ceramic Society* 99, no. 4 (2016): 1367-1374. <https://doi.org/10.1111/jace.14084>
- [31] Greco, Sebastian, Kevin Gutzeit, Hendrik Hotz, Benjamin Kirsch, and Jan C. Aurich. "Selective laser melting (SLM) of AISI 316L—impact of laser power, layer thickness, and hatch spacing on roughness, density, and microhardness at constant input energy density." *The International Journal of Advanced Manufacturing Technology* 108 (2020): 1551-1562. <https://doi.org/10.1007/s00170-020-05510-8>
- [32] Ammosova, Lena, Santiago Cano Cano, Stephan Schuschnigg, Christian Kukla, Kari Mönkkönen, Mika Suvanto, and Joamin Gonzalez-Gutierrez. "Effect of metal particle size and powder volume fraction on the filling performance of powder injection moulded parts with a microtextured surface." *Precision Engineering* 72 (2021): 604-612. <https://doi.org/10.1016/j.precisioneng.2021.06.014>
- [33] Sattari, S., M. Jahani, and A. Atrian. "Effect of volume fraction of reinforcement and milling time on physical and mechanical properties of Al₇₀Si₃₀ composites fabricated by powder metallurgy method." *Powder Metallurgy and Metal Ceramics* 56, no. 5-6 (2017): 283-292. <https://doi.org/10.1007/s11106-017-9896-2>
- [34] Xuan, Lee Wei, Mohd Fadhil Majnis, Syahriza Ismail, and Mohd Azam Mohd Adnan. "Synthesis of bi-component ZrO₂/Ag nanotube for heavy metal removal." *Progress in Energy and Environment* (2021): 23-33. <https://doi.org/10.37934/progee.18.1.2333>
- [35] Hamid, Rahimah Abdul, Siti Nur Hidayah Husni, and Teruaki Ito. "Effect of Printing Orientation and Layer Thickness on Microstructure and Mechanical Properties of PLA Parts." *Malaysian Journal on Composites Science & Manufacturing* 8, no. 1 (2022): 11-23. <https://doi.org/10.37934/mjcs.8.1.1123>
- [36] Misran, Mohd Fakhur Razi, and Mohd Sarhan Othman. "Study on Mechanical Properties of Pla Printed using 3D Printer." *Journal of Advanced Research in Applied Mechanics* 59, no. 1 (2019): 10-18.